

Temperature shift of the absorption edge and Urbach tail of $\text{ZrS}_x\text{Se}_{2-x}$ single crystals

Mohamed Moustafa,^{1,2} Anke Wasnick,² Christoph Janowitz,² and Recardo Manzke²

¹College of Engineering, American University of the Middle East, Egaila, Kuwait

²Humboldt-Universität zu Berlin, Institut für Physik, Newtonstrasse 15, D-12489 Berlin, Germany

(Received 23 December 2016; revised manuscript received 26 March 2017; published 20 June 2017)

The temperature dependence of the absorption-edge energy has been determined in mixed layered transition-metal dichalcogenides of $\text{ZrS}_x\text{Se}_{2-x}$, for $x = 0.5, 1.0, 1.5,$ and 2.0 in the range of $32\text{--}300$ K. The single crystals of $\text{ZrS}_x\text{Se}_{2-x}$ samples have been grown by the chemical vapor transport technique and characterized with the help of different methods. The absorption edge is found to shift toward lower energy with increasing the temperature. The experimental spectra and the parameters that describe the temperature dependence of the absorption edges are evaluated and described in the framework of the model proposed by Manoogian and Woolley [Can. J. Phys. **62**, 285 (1984)]. The presence of the Urbach tail just below the band edge of $\text{ZrS}_x\text{Se}_{2-x}$ was observed. The steepness parameter σ and its functional temperature and composition dependence are discussed. Additionally, the values of the Urbach energies as well as the phonon energies are deduced. The obtained results support that the thermal phonon interactions and the structural and compositional disorders contribute to the Urbach tail in $\text{ZrS}_x\text{Se}_{2-x}$ crystals.

DOI: [10.1103/PhysRevB.95.245207](https://doi.org/10.1103/PhysRevB.95.245207)

I. INTRODUCTION

A great deal of interest in two-dimensional materials has appeared among the scientific community due to their remarkable properties that place them at the center of the revolution in advanced materials and their applications. The family of transition-metal dichalcogenides (TMDCs) are a class of important layered materials which have received much attention over the last few years. They cover the whole spectrum of electronic properties varying from metals and semimetals through large- and narrow-band-gap semiconductors to insulators [1–3]. They exhibit interesting physical properties with unique optical, electrical, and mechanical anisotropy properties originating from their remarkable 2D structural character [4,5]. The materials also possess unique morphology as thin, flexible, high-quality dangling-bond-free surfaces which are very suitable for thin-film epitaxial growth techniques [6,7]. Additionally, semiconducting materials of this class of compounds exhibit band-gap energies in the optimum range of the solar energy conversion. They have attracted attention for potential use in the fabrication of photoelectrochemical solar cells [8], switching and memory effects [9], and p - n junctions [10]. In modern electronics, they are proposed among other materials for the fabrication of novel high-mobility field-effect transistors [11,12].

The TMDC family crystallizes in a layered structure with a chemical formula MX_2 , where M stands for a transition metal and X for a Se, S, or Te chalcogen atom. Single crystals of TMDC are formed by stacks of X - M - X layers, where a sheet of metal atoms is sandwiched between two sheets of chalcogens. Within each layer the atoms are held together by strong covalent-ionic mixed bonds, while the bonding between the layers is of the relatively weak van der Waals type [13,14]. This 2D bonding character is found to be responsible for the marked anisotropy in a number of their properties. Crystals of such materials show a good cleavage in the direction perpendicular to the layers (c axis). This may be exploited to obtain thin single-crystal specimens needed for the measurements of the optical properties.

In this paper, we report $\text{ZrS}_x\text{Se}_{2-x}$ crystals where x varies from 0 to 2. These materials belong to group IVB with transition metal Zr and chalcogens S and Se and crystallize in a layered 1T structure in which the transition metal is octahedrally coordinated by six chalcogenide atoms [Fig. 1(a)]. The electron configuration of the transition metal Zr in the $\text{ZrS}_x\text{Se}_{2-x}$ is $4d^25s^2$ and that of both chalcogens S and Se is s^2p^4 , i.e., both missing two electrons for a filled shell. They are all semiconductors with relatively large energy gaps due to the quite weak p - d interactions. The valence band maximum is located at the Γ point and the conduction band minimum lies midway between Γ and K points of the Brillouin zone. Figure 1(b) illustrates the high-symmetry directions of the Brillouin zone (BZ) for single-crystals $\text{ZrS}_x\text{Se}_{2-x}$. Electronic band structure of the two end members of the series, i.e., ZrSe_2 and ZrS_2 , has been investigated theoretically based on calculations carried out with different methods [15–18]. Recently, Ghafari *et al.* have performed novel calculation within the Tran-Blaha modified Becke-Johnson density functional method both with and without spin-orbit interaction for both the end members in addition to ternary ZrSSe [19]. On the experimental side, Brauer *et al.* discussed the band structure but only for ZrSe_2 [20]. Most recently, we have presented a comprehensive study on the band structure of the complete series experimentally using angle-resolved photoemission spectroscopy in conjunction with the synchrotron radiation facilities [21,22].

Optical studies of the disulfides and diselenides of group IV TMDC semiconductors have been carried out by Greenaway and Nitsche [23], followed by Lee *et al.* [24] on cleaved single crystals of ZrS_2 , HfSe_2 , and HfS_2 [23] and ZrSe_2 and TiS_2 [24]. Attempts to explain the optical properties in terms of the energy-band scheme of TMDCs were given by Wilson and Yoffe [25] and by Huisman *et al.* [26]; they have later been supported by theoretical calculations and experimental data. Hughes and Liang [27] performed vacuum ultraviolet reflectivity measurements in the photon energy range from 4.5 to 14 eV of the disulfides and diselenides of group IVB compounds. Transmission spectra of group IV TMDC semiconductors have been reported [28].

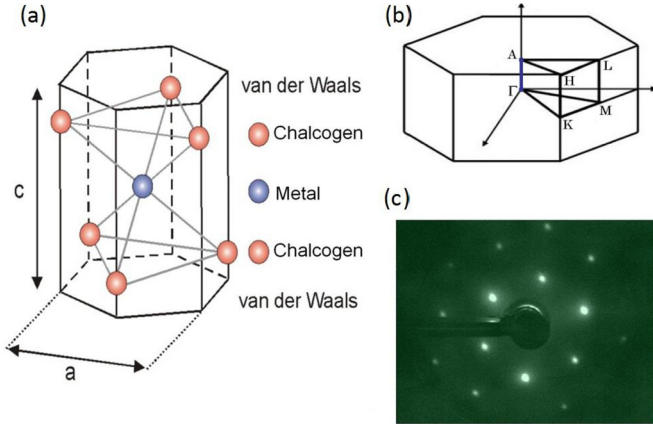


FIG. 1. (a) 1T structure with the octahedral coordinated transition metal of TMDC materials. (b) Single crystals ZrS_xSe_{2-x} corresponding Brillouin zone with the high-symmetry directions. (c) LEED pattern of ZrS_2 at electron energy of 102 eV.

However, there is not thorough work on the ternary mixed single crystals of the TMDCs. In our earlier paper, the band-gap energies for the whole series of ZrS_xSe_{2-x} at room temperature have been reported [29]. In this work, the study is extended and a detailed investigation of the fundamental absorption edge of ternary ZrS_xSe_{2-x} single crystals with compositions $x = 0.5, 1.0, 1.5,$ and 2.0 in the temperature range of 32 K to room temperature is reported. The behavior of the exponential Urbach tail and the mechanism of the thermal and nonthermal dependence of the absorption edge are discussed in detail. The Urbach rule and its importance for contemporary solid-state optical spectroscopy has been reviewed recently [30]. The characteristic Urbach parameters such as the steepness parameters σ and their temperature dependence and the deduced values of the Urbach energies and phonon energies are presented and analyzed.

II. EXPERIMENTAL METHODS

Single crystals of mixed ZrS_xSe_{2-x} used in this work were prepared utilizing the convenient chemical vapor transport technique using iodine as the transport agent [31,32]. Sulfur and selenium powders of 99.999% purity and zirconium of 99.8% purity were taken in stoichiometric proportions and placed in transparent quartz ampoules. The transporting agent iodine (purity of 99.999%) was also placed along with the powders, with concentration of 5 mg cm^{-3} of the ampoule volume. Ampoules were sealed under vacuum. The crystal growth took place in a four-zone horizontal furnace with a reaction temperature in a range of 850°C of uninterrupted heat treatment for a period of about 350 h. More details concerning the method and experimental parameters used for the crystal growth can be found in [29]. The crystals obtained by this technique exhibit sizes up to, e.g., $20 \times 10 \text{ mm}^2$ in the superficial area. Good cleavage properties in the direction perpendicular to the c axis were obtained. No further polishing and cleaning treatments were required because of the clean mirrorlike faces. The stoichiometric compositions of the as-grown crystals were determined using energy-dispersive x-ray emission (EDX). Small deviations from the nominal

compositions have been found, which are ascribed to the nonexact stoichiometric character of the TMDC materials, in particular the case of column IV, grown by this technique [33]. The thickness of the crystals was measured by an electron microscope (Cambridge Instruments S360). For a qualitative determination of the structure, low-energy electron diffraction (LEED) was carried out; see Fig. 1(c). The measurements of the optical absorption, for all crystals, have been carried out between 32 and 300 K. For this purpose, an air product cryostat cooled by helium gas was employed to obtain the spectra at the required temperature. Transmission measurements were performed by a prism monochromator (Carl Zeiss Jena) and a high-precision digital voltmeter (Schlumberger Technologies 7071). The system was computer controlled for the data collection and storage.

III. RESULTS AND DISCUSSION

The photon energy ($h\nu$) dependence of the absorption coefficient (α) is expressed, after approximation for a case of sufficiently high value of (αd), where d is the sample thickness, according to [34]

$$\alpha(\lambda) \cong \frac{1}{d} \{-\ln T(\lambda) + 2 \ln(1 - R(\lambda))\}, \quad (1)$$

where T and R are the transmittance and the reflection loss, respectively. Transmittance ratios were measured for four different compositions of the mixed single crystals of ZrS_xSe_{2-x} for $x = 0.5, 1.0, 1.5,$ and 2.0 at a number of stabilized temperatures between 20 and 300 K for samples with thickness variation between $1.8 \mu\text{m}$ for $x = 0.5$ and $5.8 \mu\text{m}$ for $x = 2.0$. The required small thickness for $ZrSe_2$ prevented us from carrying out measurements for this sample. The absorption coefficient has been determined using Eq. (1) after properly correcting for the reflection. For the case of $ZrS_{1.5}Se_{0.5}$ sample, the variation of the absorption coefficient at two different temperatures is shown in Fig. 2(a). The absorption edge shifts toward lower energy with increasing temperature. For optical characterization, the band-gap values of the samples were determined by analyzing the energy

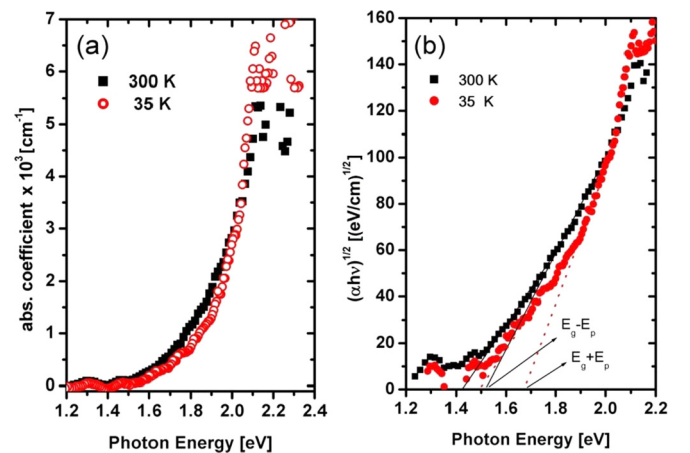


FIG. 2. For $ZrS_{1.5}Se_{0.5}$ sample: (a) Plot of the absorption coefficient in the range of the energy gap at 35 and 300 K. (b) $(\alpha h\nu)^{1/2}$ vs the photon energy ($h\nu$), extrapolating the linear part of each curve toward energy axis gives the corresponding energy-gap value.

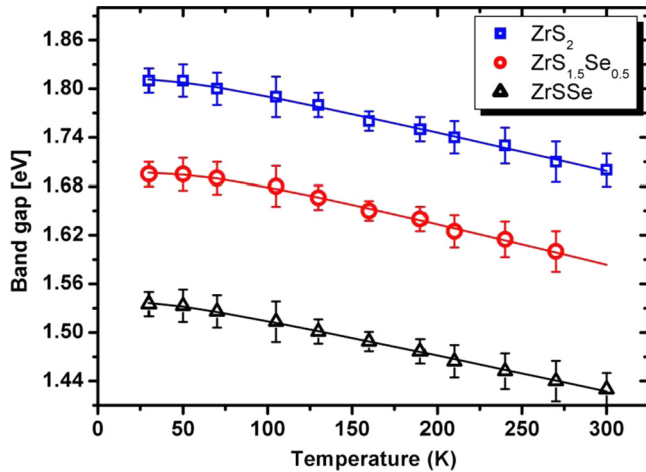


FIG. 3. Band-gap energy as a function of temperature of ZrS_xSe_{2-x} . Points represent the experimental deduced E_g at different temperature. The solid line is the fitting according to Eq. (3).

dependence of the absorption coefficient $\alpha(h\nu)$ for indirect allowed transitions, taking into account the absorption and emission of phonons according to $\alpha(h\nu) = C(h\nu - E_g \pm E_p)^{1/2}$ [34]. C is a temperature-independent constant, E_g is assigned to the indirect band gap, $h\nu$ is the energy of the incident photon, and E_p is the energy of the absorbed (+) or emitted (-) phonon. Figure 2(b) illustrates an example of the determination of the band-gap energy by the extrapolating $(\alpha h\nu)^{1/2}$ vs $h\nu$ curve to $(\alpha h\nu)^{1/2} = 0$. More details on the linear fit of the extrapolation of $(\alpha h\nu)^{1/2}$ for indirect allowed transitions are found in the previous work, Ref. [29]. The obtained results of the band-gap determination extracted by the above equation as a function of temperature are illustrated by points in Fig. 3 for three samples of the ZrS_xSe_{2-x} series. Multiple reflections in the zirconium films occur and cause interference fringes in both the transmittance and the reflectance data, which may be the cause of the appearance as small maxima at approximately 1.3 and 1.43 eV in the absorption edge.

For a comprehensive understanding of the obtained results, we begin with a brief review of the temperature dependence of the band gap of semiconductors. The fundamental optical absorption edge of most semiconductors and insulators exhibits a shift with temperature. The general trend is that the edge shifts to lower energy with increasing temperature, i.e., negative dE_g/dT . However, there are some cases such as lead semiconductor compounds (PbS, PbSe, and PbTe) where the edge shifts to higher energy with temperature [35], which is not realized in our case. Much work has been carried out to explain the temperature dependence of the energy gap from several approaches [36–38]. In general, there are two main attributions for the temperature dependence of the energy gap in any semiconductor [36,39]. The first reason is the *explicit* effect of the electron-phonon interaction [40], while the second one is the *implicit* lattice dilation term which is due to the thermal expansion and the consequent changes in the band structure with volume. It has been found that the latter contributes an amount on the order from 5 to 25% to the temperature shift, depending on the semiconductor. However, the former one represents the dominant participation of the temperature-

dependence shift. Many experimental studies have confirmed this assignment [36,41]. The lattice dilation behavior can be understood if one considers that the interatomic spacing increases with temperature when the amplitude of the atomic vibrations about their equilibrium position increases, due to the increased thermal energy. This effect is quantified by the linear expansion coefficient of a material. An increase in the interatomic spacing leads to a decrease in the potential seen by the electrons in the material, which in turn reduces the size of the energy band gap [34].

The explicit term due to electron-phonon interaction at constant volume is usually the more difficult one to evaluate and it has challenged theorists for many years [38,41]. However, a number of semiempirical relations have been proposed to express the variation of the band gap with temperature in semiconductors. The earliest and much commonly used relation for this band-gap temperature dependence of semiconductors is the one proposed by Varshni [42]. It has satisfactorily described the experimental data for a number of semiconductors such as C, Si, and Ge, and it was later used for some layered mixed semiconductors [43]. In spite of this, it has some drawbacks related to the Debye temperature, which may in certain cases be negative [44]. Moreover, at low temperatures the Varshni equation predicts a quadratic band-gap dependence with temperature whereas experiments have found an approximate temperature independence at very low temperatures. Additionally, if the Varshni equation is used to describe the complete energy-gap variation, then it is implied that the effect of lattice dilation has been lumped into the electron-phonon term. These points have been noted by Manoogian and Woolley [44] and another semiempirical equation has been proposed. In their approach it is assumed that $\Delta E = E_g(T) - E_g(0) = 0$ at $T = 0$ K. The variation of E_g with T is given by [44]

$$E_g(T) = E_g(0) - UT^s - V\Theta [\coth(\Theta/2T) - 1], \quad (2)$$

where $E_g(0)$ is the band gap at 0 K, U , s , and V are parameters independent of temperature, and Θ is the mean frequency of phonon excitation. It is related to the Debye temperature through $\Theta \approx 3/4 \Theta_D$ [45]. It permits, therefore, an evaluation of the effect of the lattice dilation term and the electron-phonon interaction term separately. It has also been shown that the Varshni equation is a second-order approximation of the electron-phonon term in the proposed equation of Manoogian and Woolley [Eq. (2)]. Comparison with experimental data for many semiconductors has been carried out and showed in general a very good agreement with the foregoing proposed expression.

Values of the parameters $E_g(0)$, U , V , and Θ , obtained by fitting $E_g(T)$ data of Fig. 4 to Eq. (2), are given in Table I. It can be observed that at higher temperature it is almost linear with T . Since the best fit to the data was achieved with s very close to 1, in the final adjustment we have used $s \approx 1$. For ZrS_2 , the value of $\Theta = (143.7 \pm 11)$ K obtained from a fit of the E_g vs T data to Eq. (3) gives a value for $\Theta_D = (191.6 \pm 11)$ K. The Debye temperature can also be estimated from the Lindemann formula [45]:

$$\Theta_D \simeq 120 T_m^{1/2} A^{-5/6} \rho^{1/3}, \quad (3)$$

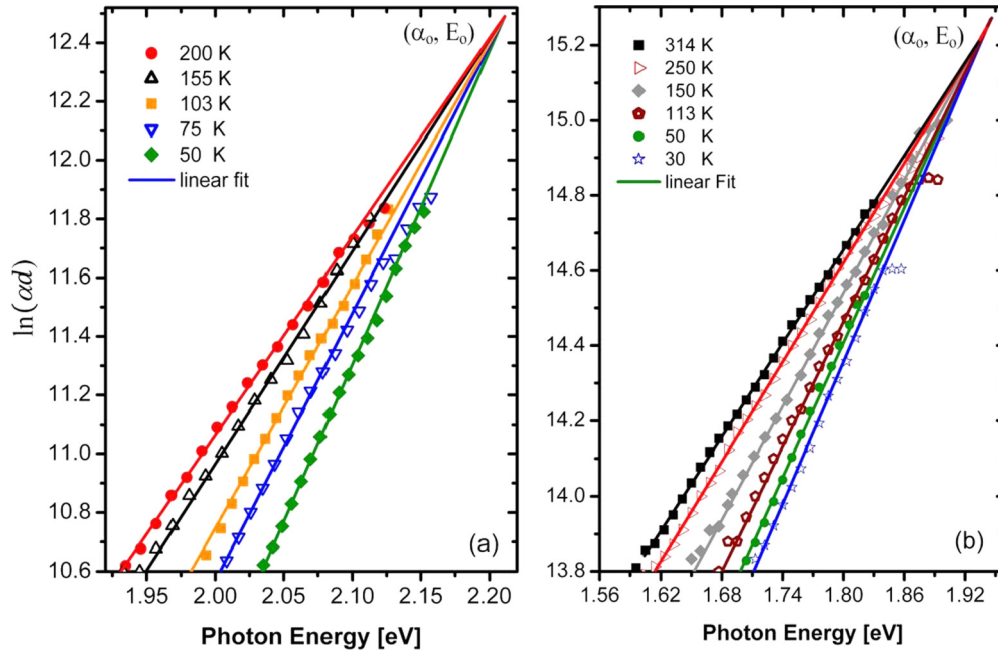


FIG. 4. $\ln(\alpha d)$ vs the photon energy $h\nu$ for a ZrS_2 (a) and a $\text{ZrS}_{0.5}\text{Se}_{1.5}$ (b) single crystal. The solid lines represent the best linear fit of the measured data. A good approximation to a linear temperature dependence is observed, consistent with Eq. (6). (α_0, E_0) is referred to as the corresponding converging point (or Urbach focus).

where T_m is the melting point, A is the mean atomic weight, and ρ is the mean density of the material. ZrS_2 decomposes without melting at a temperature of 1480°C [46]. Therefore, taking this to be the decomposition temperature T_m in Eq. (4) with $A = 155.35$ g/mol and $\rho = 3.87$ g/cm³ [46] leads to $\Theta_D \approx 140$ K. The value of Θ_D estimated using the Lindemann formula agreed well with that derived from the fitted parameter. Further, the contribution of the lattice dilation, the implicit term, of the variation of the energy gap with temperature in a semiconductor can be estimated as

$$\left. \frac{\partial E_g}{\partial T} \right|_{LD} = \left. \frac{\partial E_g}{\partial V} \right|_T \left. \frac{\partial V}{\partial T} \right|_P \simeq -\frac{\gamma}{\beta} (\partial E_g / \partial P), \quad (4)$$

where γ , β , and $(\partial E_g / \partial T)$ are the isobaric volume dilation coefficient, the isothermal compressibility, and the pressure coefficient of the energy gap, respectively [14]. γ for the layered compounds is $3\alpha_L$, where α_L is the linear thermal expansion coefficient and is modified for layered materials to $[1/3(2\alpha_{\parallel} + \alpha_{\perp})]$ and β to $[1/3(2\beta_{\parallel} + \beta_{\perp})]$ [47,48]. The subscripts indicate directions along and perpendicular to

TABLE I. Values of the band gap at 0 K, $E_g(0)$, and the parameters U , V , and Θ according to Eq. (3), obtained from a fit of the experimental temperature dependence of E_g , for several compounds of the $\text{ZrS}_x\text{Se}_{2-x}$ crystal. Parameter s is taken ≈ 1 .

$\text{ZrS}_x\text{Se}_{2-x}$	Thickness x	$E_g(0)$ (eV)	U ($\times 10^{-4}$ eV/K)	V ($\times 10^{-5}$ eV/K)	Θ (K)
0.5	1.8	1.422	3.50	4.0	200.5
1.0	3.4	1.536	3.05	3.1	190.0
1.5	5.8	1.696	2.10	2.4	184.2
2.0	4.8	1.812	1.04	2.5	144.7

the crystal layers. Values of the expansion coefficient and compressibility are greater along the c -axis direction than that of the direction parallel to the layers. This is attributed to the easy reduction in the van der Waals gap between successive MX_2 sandwiches. Using the reported value for ZrS_2 of $\gamma = 1.15 \times 10^{-5} \text{ K}^{-1}$ from [48], $\beta \approx 6 \times 10^{-12} \text{ Pa}^{-1}$ and $(\partial E_g / \partial P) \approx 5 \times 10^{-11} \text{ eV/Pa}$ from [47], leads to a lattice dilation term U in Eq. (3) of $\sim 1.03 \times 10^{-4} \text{ eV K}^{-1}$ which is in good agreement with the value given in Table III. However, for mixed compositions, similar evaluations cannot be considered as there are no data available. Nevertheless the obtained experimental results show the expected trend. Thermal expansion coefficients for some common layered TMDC materials, collected from [49], are given in Table II. The values are larger along the perpendicular direction compared to the values along the parallel direction, which is attributed to the weak van der Waals (vdW) forces. Substitution of S by Se shows higher values, which leads to an increase in the thermal lattice dilation term. The β is smaller in ZrSe_2 than in ZrS_2 .

TABLE II. Linear thermal expansion coefficients α for ZrS_2 and other TMDCs, from [48]. Subscripts indicate directions along and perpendicular to the crystal layers.

Compound	Temperature range ($^\circ\text{C}$)	α_{\parallel} [$\times 10^{-5}$ ($^\circ\text{C}$) ⁻¹]	α_{\perp} [$\times 10^{-5}$ ($^\circ\text{C}$) ⁻¹]
ZrS_2	23–500	1.00 ± 0.02	1.45 ± 0.02
SnS_2	23–550	0.95 ± 0.02	1.35 ± 0.01
SnSe_2	23–390	1.33 ± 0.02	1.74 ± 0.01
SnSSe	23–380	1.75 ± 0.02	1.94 ± 0.01
HfS_2	23–735	0.34 ± 0.03	0.93 ± 0.02
TiS_2	23–590	1.51 ± 0.02	1.90 ± 0.01

Notice that ZrSe_2 is denser than ZrS_2 with density values of 5.36 and 3.72 g/cm³, respectively. The γ of ZrSe_2 is higher than that of ZrS_2 , as the c/a ratios of ZrSe_2 and ZrS_2 are 1.627 and 1.586, respectively. As such, the lattice dilation contribution for Se-rich compositions is expected to be higher than that of S-rich compositions. This gives an explanation of the observed general experimental trend for the ternary $\text{ZrS}_x\text{Se}_{2-x}$ compounds as moving from ZrSe_2 toward ZrS_2 , which is given in Table I.

The measured samples over the whole compositional range have shown an absorption tail below the absorption coefficient, well known as ‘‘Urbach’s tail’’ [50]. Extensive theoretical studies and a large number of experimental investigations have been launched to explain the origin of this tail. For example, Sumi and Toyozawa [51] and Abay *et al.* [52] attribute the absorption tail to the interaction of electrons and excitons with phonons in the semiconductors. Cody *et al.* [53] and Ho *et al.* [54] suggest that the residual absorption below the absorption edge most probably originates from the temperature-independent imperfections of the material and static disorder and indicates the existence of impurities, dislocations, stacking faults, etc. in the layered materials. It has been found that the Urbach tail obeys the expression [50]

$$\alpha = \alpha_o \exp\left(\frac{E - E_o}{E_U}\right), \quad (5)$$

where α_o and E_o are characteristic parameters of the material. $E = \hbar\omega$ and E_U are the photon energy and the so-called Urbach energy, respectively.

According to Eq. (5) a plot of the natural logarithm of the measured absorption coefficient ($\ln \alpha$) against the photon energy ($\hbar\nu$) near the absorption edge yields to an approximately straight line for energies just below the fundamental absorption edge. This is indeed what it is found. Figures 4(a) and 4(b) represent the plot for ZrS_2 and $\text{ZrS}_{0.5}\text{Se}_{1.5}$, respectively. A very good fit of the absorption edge for the crystals of some compositions at different temperatures (solid lines in Fig. 4) to the experimental results is obtained. The Urbach energy for the crystals at different temperatures were calculated from the slope of the straight lines in Fig. 4. Two other Urbach parameters (α_o , E_o), which are independent of the temperature, referred to as the converging point (or Urbach focus), have been obtained from the linear extrapolations of ($\ln \alpha$) vs ($\hbar\nu$) plot. E_o is found to be indicative of the energy value of the absorption edge below which the Urbach tail extends. Similar analysis has been carried out for the three other measured samples and the values of E_o and α_o are collected in Table III. In Eq. (5) the Urbach energy is expressed as $E_U = k_B T / \sigma$, where k_B is the Boltzmann constant, T is the absolute temperature, and σ is the so-called steepness parameter, which characterizes the steepness (inverse of the slope) or the width of the straight line near the absorption edge. The steepness parameter σ has the following temperature dependence [55]:

$$\sigma = \sigma_o \frac{2k_B T}{\hbar\omega_o} \tanh \frac{\hbar\omega_o}{2k_B T}, \quad (6)$$

where σ_o is a temperature-independent but material-dependent parameter and $\hbar\omega_o$ has been found experimentally to fit the energies of the phonons in the crystal; k_B and T have the

TABLE III. Values of the characteristic Urbach tail parameters σ_o and $\hbar\omega_o$ deduced from the fitting of the experimental results according to Eq. (6). The determined converging point (α_o , E_o) for the $\text{ZrS}_x\text{Se}_{2-x}$ series.

$\text{ZrS}_x\text{Se}_{2-x}$ x	σ_o	$\hbar\omega_o$ (meV)	α_o ($\times 10^6 \text{ cm}^{-1}$)	E_o (eV)
0.5	0.151	52.4	3.9	1.94
1.0	0.155	42.2	3.1	1.98
1.5	0.162	40.5	2.2	2.05
2.0	0.164	37.2	0.3	2.21

same meanings as above. This formula can be used to estimate the type and the energy of the phonons taking part in this process. The steepness parameter σ at different temperatures has been calculated from the slope of the lines (of Fig. 4). The deduced steepness parameter values σ are plotted as a function of temperature as shown in Fig. 5 for $\text{ZrS}_{0.5}\text{Se}_{1.5}$ and ZrS_2 , in comparison with theoretical graphs that are based on Eq. (6). It is observed that σ_o increases with increasing temperature, clearly at high temperatures it is very close to σ_o . The values of σ_o and $\hbar\omega_o$ have been calculated as fitting parameters for each curve. The material parameter σ_o is found to increase from rich selenium to sulfur. The composition dependence of the parameter σ_o is discussed in detail below. Phonon energy values $\hbar\omega_o$ of 52.2 ± 0.2 and 37.2 ± 0.2 meV have been estimated for $\text{ZrS}_{0.5}\text{Se}_{1.5}$ and ZrS_2 , respectively. These values are in the same range as earlier reported data of similar compounds and also of other layered indirect semiconductors [56,57].

The temperature dependence of the steepness parameter is used to determine the physical origin of the Urbach tail in the absorption process. In the approach considered under the assumption that the dominant cause for the Urbach tail is the exciton-phonon interaction, σ is temperature dependent according to Eq. (6). The theoretical treatment of this slope parameter was first developed for the exciton-phonon interaction in pure ionic crystals [58]. On the other hand, it has been shown that when the phonon contribution is small (low-energy phonons) and/or the crystals are not chemically homogeneous

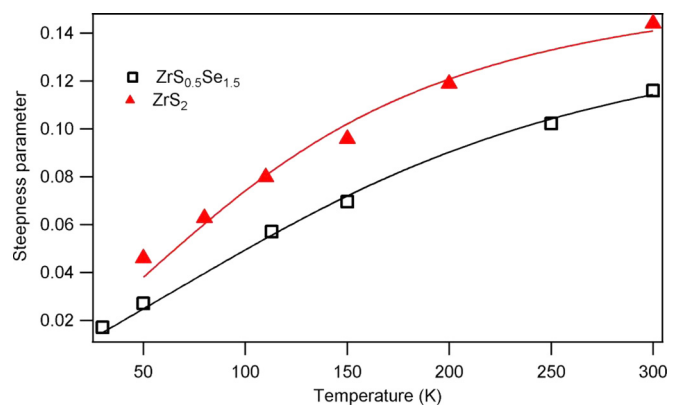


FIG. 5. Plot of the steepness parameters σ vs temperature T for ZrS_2 and $\text{ZrS}_{0.5}\text{Se}_{1.5}$ single crystals. Points represent values of σ calculated from the slope of each line at different temperatures from Fig. 3, while the solid curve represents a function fit according to Eq. (6) with fitting parameters σ_o and $\hbar\omega_o$ (values are collected in Table III).

(e.g., mixed crystals), the steepness parameter σ will shift linearly with temperature and the slope [σ/kT (in eV^{-1})] of the absorption edge is nearly independent of temperature, i.e., constant with temperature. If that is the case, the broadening of the absorption edge which gives rise to the exponential Urbach tail is mainly caused by structural disorder (e.g., from charged defects). This has been observed for direct semiconductors, and the contributions due to the defects prevail and the phonon contribution is obscured (see for example [59] for some ternary semiconductors). The above discussion, and according to the obtained temperature dependence of the slope parameter σ , leads to a conclusion that this is a manifestation of the electron/exciton-phonon interaction influence on the absorption coefficient. Nevertheless, the effect of the structural disorder cannot be excluded in our case. This argument can be discussed by considering the obtained values of the steepness parameter σ as follows. The low values of σ , corresponding to relatively large values of Urbach energy E_U , suggest that besides the temperature-dependent phonon participation to the Urbach tail, there are additional nonthermal components that contribute to this tail. They are the structural and compositional disorders accompanied with nonideal single crystals. This relation between the size of the Urbach energy, consequently of σ , and the causes of this behavior has been experimentally and theoretically discussed [53], i.e., the values of E_U become larger (σ becomes lower), indicating both interaction factors rather than one. Additionally, the estimated phonon energy values $\hbar\omega_o$ for the crystals derived from the data fit according to Eq. (6) are relatively higher than the values reported in literature [$\hbar\omega_o = 37.2$ meV for ZrS_2 in comparison to ~ 32 meV [56]]. This supports the idea of contribution of the structural and compositional disorders to the absorption edge. Kranjcec *et al.* [59] and Desnica *et al.* [60] have indicated that the larger values of $\hbar\omega_o$ in the mixed crystals are due to structural disorder which could be caused by cation-cation disorder, cation vacancies, and interstitials. The increasing values of σ_o as progressing from ZrSe_2 to ZrS_2 can be attributed to the higher degree of disorders and impurities in the Se compounds than in the S compounds. This can be understood by considering the nonexact stoichiometric character accompanying the crystal growth, producing impurity-type extrinsic properties. This behavior is probably due to the 2D character of these materials where the layers are held together by relatively weak vdW forces. For the highest chalcogen content, the crystals have chalcogen vacancies in the van der Waals gap. These vacancies become progressively occupied by additional metal atoms as they are often taken up into the vacant sites in the vdW gaps

[61] and accordingly small amounts of excess metal are always present. This is the so-called self-intercalation mechanism, due to formation of Frenkel defects. The ZrSe_2 samples show more disorder (Frenkel defects) than ZrS_2 crystals; refer to [21,22]. Similar observation has been also reported for other layered semiconducting dichalcogenide composites of selenium and sulfur [56]. The previous discussion leads to the conclusion that the Urbach tail observed in the $\text{ZrS}_x\text{Se}_{2-x}$ single crystals under investigation is due to both temperature-independent static structural disorder and electron/exciton-phonon induced interactions, i.e., thermal dynamic phonon disorder. The results are consistent with the idea that the thermal and structural disorders are additive. The structural disorder is found to be dominant at low temperatures, while the contribution from both parameters becomes comparable at room temperature. Alternatively, intrinsic in-gap states originating from polaronic and charge-transfer defects have been discussed for transparent conducting oxides and other semiconductors recently [62]. However, there is no theory at present relating these intrinsic states to the Urbach tail nor do we know whether these intrinsic states exist in our material.

IV. CONCLUSIONS

The temperature dependence of the band-gap energies of the $\text{ZrS}_x\text{Se}_{2-x}$ indirect semiconductor has been determined. The variation of the energy gap with temperature is compared to the semiempirical model proposed by Manoogian-Woolley considering both the lattice dilation due to the change in the volume with temperature and the electron-phonon interactions terms separately. The absorption coefficient near the fundamental absorption edge is energy- and temperature-dependent according to the Urbach rule. The temperature dependence of the steepness parameter σ leads to a conclusion that the electrons/excitons with phonons cause the exponential Urbach tail. The low values of the σ corresponding to a large width indicate that there are additional nonthermal structural disorders associated with the existence of impurities and defects in mixed layered semiconductors. Experimental observations agree favorably with the idea that the thermal and the static disorder are additive.

ACKNOWLEDGMENTS

The authors would like to thank P. Schäfer for the EDX and electron microscope measurements. M.M. gratefully thanks for the Yousef Jameel Scholarship.

[1] R. H. Friend and A. D. Yoffe, *Adv. Phys.* **36**, 1 (1987).

[2] J. C. E. Rasch, T. Stemmler, B. Müller, L. Dudy, and R. Manzke, *Phys. Rev. Lett.* **101**, 237602 (2008).

[3] W. S. Yun, S. W. Han, S. C. Hong, I. G. Kim, and J. D. Lee, *Phys. Rev. B* **85**, 033305 (2012).

[4] R. Manzke and M. Skibowski, in *Photoelectron Spectra of Layered Compounds*, Landolt-Börnstein, New Series, Group III, edited by A. Goldmann, Vol. 17B, Pt. 84 (Springer-Verlag, Berlin, 1994).

[5] C. Gaiser, T. Zandt, A. Krapf, R. Serverin, C. Janowitz, and R. Manzke, *Phys. Rev. B* **69**, 075205 (2004).

[6] K. Saiki, K. Ueno, T. Shimada, and A. Koma, *J. Cryst. Growth* **95**, 603 (1989).

[7] A. Koma, *J. Cryst. Growth* **201-202**, 236 (1999).

[8] H. Tributsch, *Appl. Phys. (Berlin)* **23**, 61 (1980).

[9] E. Bucher, in *Photoelectrochemistry and Photovoltaics of Layered Semiconductors*, edited by A. Aruchamy (Kluwer Academic, Dordrecht, 1992), pp. 1–81.

- [10] R. Späh, U. Elrod, M. Lux-Steiner, E. Bucher, and S. Wagner, *Appl. Phys. Lett.* **43**, 79 (1983).
- [11] V. Podzorov, M. E. Gershenson, C. Kloc, R. Zeis, and E. Bucher, *Appl. Phys. Lett.* **84**, 3301 (2004).
- [12] D. Jiménez, *Appl. Phys. Lett.* **101**, 243501 (2012).
- [13] A. D. Yoffe, *Solid State Ionics* **39**, 1 (1990).
- [14] M. P. Deshpande, P. D. Patel, M. N. Vashi, and M. K. Agarwal, *J. Cryst. Growth* **197**, 833 (1999).
- [15] D. W. Bullett, *J. Phys. C* **11**, 4501 (1978).
- [16] H. M. Isomaki, J. von Boehm, and P. Krusius, *J. Phys. C* **12**, 3239 (1979).
- [17] A. H. Reshak and S. Auluck, *Physica B* **353**, 230 (2004).
- [18] H. Jiang, *J. Chem. Phys.* **134**, 204705 (2011).
- [19] A. Ghafari, A. Boochani, C. Janowitz, and R. Manzke, *Phys. Rev. B* **84**, 125205 (2011).
- [20] H. E. Brauer, H. I. Starnberg, L. J. Holleboom and H. P. Hughes, *J. Phys.: Condens. Matter* **7**, 7741 (1995).
- [21] M. Moustafa, A. Ghafari, A. Paulheim, C. Janowitz, and R. Manzke, *J. Electron Spectrosc. Relat. Phenom.* **189**, 35 (2013).
- [22] M. Moustafa, A. Paulheim, M. Mohamed, C. Janowitz, and R. Manzke, *Appl. Surf. Sci.* **366**, 397 (2016).
- [23] D. L. Greenaway and R. Nitsche, *J. Phys. Chem. Solids* **26**, 1445 (1965).
- [24] P. A. Lee, G. Said, R. Davis, and T. H. Lim, *J. Phys. Chem. Solids* **30**, 2719 (1969).
- [25] J. A. Wilson and A. D. Yoffe, *Adv. Phys.* **18**, 193 (1969).
- [26] R. Huisman, R. de Jonge, C. R. Haas, and F. Jellinek, *J. Solid State Chem.* **3**, 56 (1971).
- [27] H. P. Hughes and W. Y. Liang, *J. Phys. C: Solid State Phys.* **10**, 1079 (1977).
- [28] A. R. Beal, J. C. Knights, and W. Y. Liang, *J. Phys. C: Solid State Phys.* **5**, 3531 (1972).
- [29] M. Moustafa, T. Zandt, C. Janowitz, and R. Manzke, *Phys. Rev. B* **80**, 035206 (2009).
- [30] I. Studenyak, M. Kranjec, and M. Kurik, *Int. J. Opt. Appl.* **4**, 76 (2014).
- [31] C. R. Whitehouse, H. P. B. Rimmington, and A. A. Balchin, *Phys. Status Solidi* **18**, 623 (1973).
- [32] F. A. S. Al-Alamy and A. A. Balchin, *J. Cryst. Growth* **39**, 275 (1977).
- [33] C. R. Whitehouse and A. A. Balchin, *Phys. Status Solidi* **47**, K173 (1978).
- [34] J. I. Pankove, *Optical Processes in Semiconductors* (Dover, New York, 1971).
- [35] N. M. Ravindra and V. K. Srnasta, *Phys. Status Solidi* **58**, 311 (1980).
- [36] P. B. Allen and M. Cardona, *Phys. Rev. B* **27**, 4760 (1983).
- [37] K. P. O'Donnell and X. Chen, *Appl. Phys. Lett.* **58**, 2924 (1991).
- [38] S. Biernacki, U. Scherz, and B. K. Meyer, *Phys. Rev. B* **49**, 4501 (1994).
- [39] F. Abelès, *Optical Properties of Solids* (North-Holland, Amsterdam, 1972).
- [40] G. Lucovsky, R. M. White, J. A. Benda, and J. F. Revelli, *Phys. Rev. B* **7**, 3859 (1973).
- [41] K. W. Böer, *Survey of Semiconductor Physics*. (Van Nostrand Reinhold, New York, 1990).
- [42] Y. P. Varshni, *Physica* **34**, 149 (1967).
- [43] S. Y. Hu, Y. C. Lee, J. L. Shen, K. W. Chen, K. K. Tiong, and Y. S. Huang, *Solid State Commun.* **139**, 176 (2006).
- [44] A. Manoogian and J. C. Woolley, *Can. J. Phys.* **62**, 285 (1984).
- [45] J. M. Ziman, *Electrons and Phonons: The Theory of Transport Phenomena in Solids* (Clarendon, Oxford, 1960).
- [46] D. R. Lide, *CRC Handbook of Chemistry and Physics*, 85th ed. (Taylor & Francis, CRC Press, Boca Raton, FL, 2004).
- [47] A. J. Grant, J. A. Wilson, and A. D. Yoffe, *Philos. Mag.* **25**, 625 (1972).
- [48] L. Roubi and C. Carlone, *Can. J. Phys.* **66**, 633 (1984).
- [49] F. A. S. Al-Alamy, A. A. Balchin, and M. White, *J. Mater. Sci.* **12**, 2037 (1977).
- [50] F. Urbach, *Phys. Rev.* **92**, 1324 (1953).
- [51] H. Sumi and Y. Toyozawa, *J. Phys. Soc. Jpn.* **31**, 342 (1971).
- [52] B. Abay, H. S. Güder, H. Efeoğlu, and Y. K. Yoğurtçu, *J. Appl. Phys.* **84**, 3872 (1998).
- [53] G. D. Cody, T. Tiedje, B. Abeles, B. Brooks, and Y. Goldstein, *Phys. Rev. Lett.* **47**, 1480 (1981).
- [54] C. H. Ho, Y. S. Huang, K. K. Tiong, and P. C. Liao, *Phys. Rev. B* **58**, 16130 (1998).
- [55] M. V. Kurik, *Phys. Status Solidi* **8**, 9 (1971).
- [56] K. Terashima and I. Imai, *J. Phys. Soc. Jpn.* **59**, 738 (1990).
- [57] B. Abay, H. S. Güder, H. Efeoğlu, and Y. K. Yoğurtçu, *J. Phys. Chem. Solids* **62**, 747 (2001).
- [58] H. Mahr, *Phys. Rev.* **132**, 1880 (1963).
- [59] Y. Kranjcec, D. I. Desnica, B. Čelustka, G. S. Kovacs, and I. P. Studenyak, *Phys. Status Solidi* **144**, 223 (1994).
- [60] D. I. Desnica, M. Kranjcec, and B. Čelustka, *J. Phys. Chem. Solids* **52**, 915 (1991).
- [61] J. J. Barry, H. P. Hughes, P. C. Klipstein, and R. H. Friend, *J. Phys. C: Solid State Phys.* **16**, 393 (1983).
- [62] J. Haerberle, S. Machulik, C. Janowitz, R. Manzke, D. Gaspar, P. Barquinha, and D. Schmeißer, *J. Appl. Phys.* **120**, 105101 (2016), and references therein.